Available online at www.sciencedirect.com
SCIENCE DIRECT
Journal of Sound and Vibration 296 (2006) 777–796
JOURNAL OF SOUND AND VIBRATION
www.elsevier.com/locate/jsvi

Flow-induced vibrations of an elastic cylindrical shell conveying a compressible fluid

S.V. Sorokin[a,*], A.V. Terentiev[b]

[a]Institute of Mechanical Engineering, Aalborg University, Pontoppidanstraede 101, DK 9220, Aalborg, Denmark
[b]Department of Engineering Mechanics, State Marine Technical University of St. Petersburg, St. Petersburg, 190008, Russia

Received 16 September 2004; received in revised form 2 March 2006; accepted 7 March 2006
Available online 23 May 2006

Abstract

The paper addresses the effects of generation and transmission of the vibro-acoustic energy in an elastic cylindrical shell filled with water. The energy input is produced by velocity and pressure pulsations due to the presence of an obstacle in a flowing fluid. It is assumed that there is no back-reaction of the vibro-acoustic response on the driving turbulent field. The concept of modal Green's functions and modal boundary integral equations is introduced and the role of elastic deformations of a tube is highlighted in view of the energy re-distribution between the structural and the acoustical transmission paths. Another important aspect of the problem of 'flow-induced sound generation', which is addressed in this paper, is the treatment of a CFD pressure output for the modelling of vibro-acoustic field generation. For an elastic shell in heavy fluid loading conditions, it is indicated that only the pressure distribution at the surface of a shell provided by a CFD solver is requested in order to adequately predict its coupled vibro-acoustic response. The 'inner' and 'outer' acousto-elastic domains are introduced and the low-order system of linear algebraic equations is set up, which is constituted by modal boundary equations and continuity conditions. Several 'generic' excitation cases are studied and the results of analysis are explained.

1. Introduction

The problem of flow-induced noise is one of the 'hot' topics in modern aeroacoustics. The growing demand to reduce the noise level of aircraft stimulates research into sound radiation by turbulent flow. The general trend in the modern publications in this subject is to combine codes in computational fluid dynamics (CFD) and codes in computational aeroacoustics (CAA) into a unified general tool, which enables engineers to estimate the sound radiation from various devices and subsequently to optimise their noise characteristics. In this context, classical concepts, such as, for example, Lighthill's acoustic analogy are critically revised and in effect replaced by the alternative formulations (see, for example, Proceedings of the Euromech Colloquium on this subject [1]). Probably, the most typical alternative is related to the 'sub-domain' concept, when a full system of nonlinear Navier–Stokes equations is solved, e.g., in the vicinity of a jet and its solution is matched

*Corresponding author. Tel.: +45 9635 9332; fax: +45 9815 1675.
E-mail address: svs@ime.aau.dk (S.V. Sorokin).

0022-460X/$ - see front matter © 2006 Elsevier Ltd. All rights reserved.
doi:10.1016/j.jsv.2006.03.028

Nomenclature

c_{fl}	sound speed in a fluid
E	Young's modulus
f	frequency of excitation
h	thickness of a tube
$J(\kappa\, r)$	Bessel's functions
k	root of the dispersion equation
m	circumferential number
M	number of terms retained in the modal decomposition
N_1	power flow to the right from the excitation zone
N_2	power flow to the left from the excitation zone
p	pressure in a fluid
q_3	radial component of structural excitation
Q	generalised forces
r_{ex}	location of dipole sources from its axis
R	radius of a tube
T	components of Lighthill's stress tensor
(u,v,w)	components of the vector of displacements of the shell in the axial, circumferential and radial directions, respectively
γ	ratio of Young's modulus of inner layer to the one of outer layer
Γ	volume sources
δ	Delta function
θ	circumferential angle
λ, μ	unknowns in decomposition of velocity potential
ρ_{sh}	density of structure
ρ_{fl}	density of fluid
Φ	shape of Green function
ψ	eigenmode of the distribution of a velocity potential
ω	circular frequency of excitation

Subscripts

i, m	vector entry designation, matrix row designation
j, n	matrix column designation

to the acoustic formulation (for example, in terms of the Kirchhoff integral) in the rest of a volume occupied by a compressible fluid. The underlying idea of such an approach is to identify the acoustic sources in the course of the CDF analysis 'numerically' and to 'convey' (also by means of solving the problem in fluid dynamics for a viscous compressible fluid) this 'acoustic information' onto the 'reading surface' (or, as is discussed in Ref. [2] into the 'interface layer'), where this CFD output is inserted into the purely acoustic formulation. The challenges and the advances in implementing this strategy are reported in numerous publications and it is not the aim of the present paper to pursue this subject any further.

Probably, this strategy of solving the problem in flow-induced noise is indeed the most prominent one when the high-speed flow and hot jet effects are concerned. However, there is another practical application, which may reliably be considered by a use of the 'classic' tool offered by Lighthill's acoustic analogy. This application is flow-induced noise and vibration of pipelines, where the noise is generated either by a pump or by a valve. There are several features of these industrial applications which make them substantially different from the standard problem of fan noise or turbine noise in aeroacoustics. Firstly, the Mach number of the flow is negligibly small, so that the role of convective terms in formulation of a sound and vibration field may reliably be ignored. Secondly, all effects of thermodynamics are essentially negligible. Thirdly, the operational frequency range is fairly low, $\omega R/c_{\mathrm{fl}} < 1$ (ω is a circular frequency of excitation, R is the radius of a tube, C_{fl} is the sound sped in a fluid). Finally, the role of the elastic tube, specifically, of its vibrations and waveguide properties, becomes of crucial importance in assessment of the noise transportation phenomena. This paper concerns exactly this application.

In what follows, Lighthill's equation [3] is used to describe volume sources in a fluid, and structural dynamics is described within the general theory of thin elastic shells [4] specialised for the case of heavy fluid loading. It is assumed that the flow analysis is performed within the framework of a model of viscous incompressible fluid and that there is no back-reaction of the vibro-acoustic response on the driving turbulent field. The CFD-predicted pressure fluctuations at the shell surface are regarded as the mechanical excitation of an elastic shell under heavy fluid loading, rather than as a dipole source distribution in an acoustic duct. The

methodology of boundary integral equations is used to determine the coupled structural-acoustic response of fluid-filled shell.

The paper is structured as follows. In Section 2, the governing equations are presented. The formulation of modal Green's functions is discussed in Section 3 for a cylindrical acoustical duct and for a fluid-filled elastic shell. The comparison of the energy flows in different excitation conditions specified by modal Green's matrices is performed in Section 4. In Section 5, the boundary integral equations are presented. Results of analysis of the vibro-acoustic response of an elastic tube conveying fluid with a flow obstacle are discussed in Section 6 for two generic excitation cases. The energy transmission in a compound shell is also considered.

2. The governing equations

An infinitely long elastic cylindrical shell is filled with a compressible fluid, which flows at a very low Mach number and the presence of a flow obstacle generates the coupled vibro-acoustic excitation of this structure. The standard approach to formulate this problem is related to the so-called light fluid loading case, in which the shell's wall is modelled as an absolutely rigid boundary [5,6]. Then two sources of acoustical excitation are considered. The dipole-type excitation is produced by the pressure pulsations at the surface of a flow obstacle. If this obstacle is acoustically compact, it may be replaced by a point dipole and its amplitude is determined as a net force exerted by the fluid at the obstacle, which is reciprocated back to the fluid. The quadrupole-type excitation is generated by vortex shedding from the obstacle in the wake. In the framework of this problem formulation, the energy is transmitted from the excitation zone to a far field only in an acoustic medium.

This model is perfectly valid to study, for example, the air-borne sound in ventilation tubes. However, it needs some revision in the case of an elastic cylindrical shell with heavy fluid loading—for example, when a thin metallic or polymer tube filled with water is considered, i.e., when the structural energy transmission path cannot be ignored [7]. Physically, the necessity to revise this model is explained by the fact that in the low-frequency domain the waves, which propagate in an elastic fluid-filled cylindrical shell, are of dominantly structural type so that most of the energy is actually conveyed in the structure with a relatively minor participation of the fluid. In such a structure, only one axi-symmetric ('breathing') propagating wave exists, which does not follow this rule. However, this 'fluid-originated' axi-symmetric duct wave is always accompanied by other propagating waves, which are 'structure-originated', so that the energy distribution between them is strongly dependent on excitation conditions.

It is also important to observe the substantial difference between air and water in respect to transmission of the pressure exerted by an obstacle in a near field. Water is a 'weakly compressible' acoustic medium (as compared with air) and it is able to transmit the pressure fluctuations from the flow obstacle onto the shell's wall almost instantaneously [8]. This feature manifests itself in numerical CFD analysis by the strong influence of the distance from an obstacle to the rigid wall boundary on the CDF-predicted pressure field. Therefore, for a water-filled tube in a low-frequency range it is realistic to suggest that all pressure, which is exerted on water by the obstacle, is transmitted onto the wall of a tube as if the fluid is incompressible. Then it is possible to ignore the presence of a flow obstacle in the analysis of the vibro-acoustic response and to regard the 'CFD pressure' at the surface of a shell as a mechanical excitation. This approximation is particularly relevant because the standard CFD codes operate with the 'rigid wall' boundary conditions. Of course, such a simplification is acceptable only in the low-frequency range, when the obstacle is acoustically compact and the majority of travelling waves is structure-originated, but this is exactly the operational frequency range for many technical applications.

The vibro-acoustic response of a fluid-filled elastic shell is governed by the coupled system of equations for a fluid and for a shell. Lighthill's equation, which formulates the acoustic field in water, is written in cylindrical coordinates as follows (the circumferential coordinate is separated, the circumferential wavenumber m is introduced and time dependence is chosen as $\exp(-\mathrm{i}\omega t)$):

$$\frac{\partial^2 p_m}{\partial x^2}+\frac{\partial^2 p_m}{\partial r^2}+\frac{1}{r}\frac{\partial p_m}{\partial r}-\frac{m^2}{r^2}p_m+\frac{\omega^2}{c^2}p_m=-\rho_{\mathrm{fl}}\Gamma^{(m)}(x,r). \tag{1a}$$

The acoustical excitation is specified as

$$\Gamma^{(m)}(x,r) \equiv \frac{\partial^2 T_{rr}^{(m)}}{\partial r^2} - \frac{2m}{r}\frac{\partial T_{r\theta}^{(m)}}{\partial r} + 2\frac{\partial^2 T_{rx}^{(m)}}{\partial r \partial x} - \frac{m^2}{r^2} T_{\theta\theta}^{(m)} - \frac{2}{r}\frac{\partial T_{r\theta}^{(m)}}{\partial r} + \frac{\partial^2 T_{xx}^{(m)}}{\partial x^2} + \frac{2}{r}\frac{\partial T_{rr}^{(m)}}{\partial r} - \frac{1}{r}\frac{\partial T_{\theta\theta}^{(m)}}{\partial r} - \frac{2m}{r^2} T_{r\beta\theta}^{(m)} + \frac{2}{r}\frac{\partial T_{rx}^{(m)}}{\partial x}. \tag{1b}$$

The components of Lighthill's stress tensor are defined as $T_{ij}^{(m)} \equiv v_{mi} \cdot v_{mj}$, $i,j = x,r,\theta$.

Vibrations of the shell are described in the framework of the Goldenvejzer–Novozhilov thin shell theory [4]

$$-\frac{\mathrm{d}^2 u_m}{\mathrm{d}x^2} + \frac{1-\nu}{2}\frac{m^2}{R^2} u_m - \frac{1+\nu}{2}\frac{m}{R}\frac{\mathrm{d}v_m}{\mathrm{d}x} - \frac{\nu}{R}\frac{\mathrm{d}w_m}{\mathrm{d}x} - \frac{\rho\omega^2(1-\nu^2)}{E} u_m = 0, \tag{2a}$$

$$\frac{1+\nu}{2}\frac{m}{R}\frac{\mathrm{d}u_m}{\mathrm{d}x} - \frac{1-\nu}{2}\frac{\mathrm{d}^2 v_m}{\mathrm{d}x^2} + \frac{m^2}{R^2} v_m - \frac{h^2}{12}\frac{2(1-\nu)}{R^2}\frac{\mathrm{d}^2 v_m}{\mathrm{d}x^2} + \frac{h^2}{12}\frac{m^2}{R^4} v_m + \frac{m}{R^2} w_m + \frac{h^2}{12}\frac{m^3}{R^4} w_m - \frac{h^2}{12}\frac{(2-\nu)m}{R^2}\frac{\mathrm{d}^2 w_m}{\mathrm{d}x^2} - \frac{\rho\omega^2(1-\nu^2)}{E} v_m = 0, \tag{2b}$$

$$\frac{\nu}{R}\frac{\mathrm{d}u_m}{\mathrm{d}x} + \frac{m}{R^2} v_m + \frac{h^2}{12}\frac{m^3}{R^4} v_m - \frac{h^2}{12}\frac{(2-\nu)m}{R^2}\frac{\mathrm{d}^2 v_m}{\mathrm{d}x^2} + \frac{1}{R^2} w_m + \frac{h^2}{12}\frac{d^4 w_m}{dx^4} - \frac{h^2}{12}\frac{2m^2}{R^2}\frac{\mathrm{d}^2 w_m}{\mathrm{d}x^2} + \frac{h^2}{12}\frac{m^4}{R^4} w_m - \frac{\rho\omega^2(1-\nu^2)}{E} w_m = \left(q_{3m} + p_m\right)\frac{(1-\nu^2)}{Eh}. \tag{2c}$$

In these equations, (u_m, v_m, w_m) are components of the vector of displacements of the shell in the axial, circumferential and radial directions, respectively (see Fig. A1a). The structural excitation is presented here only by the radial component q_{3m}. The component p_m is introduced in Eq. (2c) as a pressure, which is generated due to the coupled vibro-acoustic response of a shell filled with an acoustic medium to the external (strictly speaking) non-acoustical excitation defined as $\Gamma^{(m)}$ and q_{3m}.

The system of Eqs. (1, 2) is accomplished by the continuity condition:

$$r = R: \quad \frac{\partial p_m}{\partial r} = \rho_{\mathrm{fl}}\omega^2 w_m. \tag{3}$$

This problem may conveniently be solved by the method of boundary integral equations. To derive these equations, Green's matrix for all types of excitation of the elastic shell with heavy internal fluid loading should be obtained.

In this paper, the energy flow in a fluid-filled shell is selected as the principal characteristic of wave propagation phenomena. The definitions of its components are given in Appendix.

3. The Green's functions for acoustical excitation

The detailed discussion of formulation of Green's matrix for the mechanical excitation of a cylindrical shell with and without heavy fluid loading is given in Ref. [9]. The full set of excitation cases considered in this reference includes an excitation by a radial unit force, by an axial unit force, by a circumferential unit force and by an axial bending moment. Here the same methodology is applied to formulate components of Green's matrix for the acoustic excitation.

3.1. An acoustic duct

A set of Green's functions is not uniquely defined and its appropriate choice is dictated by the problem formulation. Consider as a useful illustrative example an infinitely long acoustic duct of a tubular shape. Naturally, a wave motion at any circumferential wavenumber m does not interact with wave motions at all other wavenumbers because the problem in acoustics is linear.

The 'standard' Green's function is a solution of the following equation:

$$\frac{\partial^2\hat{\Phi}_m(x,\xi,r,\hat{r})}{\partial x^2}+\frac{1}{r}\frac{\partial\hat{\Phi}_m(x,\xi,r,\hat{r})}{\partial r}+\frac{\partial^2\hat{\Phi}_m(x,\xi,r,\hat{r})}{\partial r^2}+\left[\frac{\omega^2}{c_{\mathrm{fl}}^2}-\frac{m^2}{r^2}\right]\hat{\Phi}_m(x,\xi,r,\hat{r})=\frac{1}{\hat{r}}\delta(x-\xi)\delta(r-\hat{r}). \tag{4a}$$

The right-hand side of this equation models a ring source located at $r=\hat{r}$ and $x=\xi$ with the circumferential intensity of $\cos m\theta/\hat{r}$ (θ is the circumferential angle).

The boundary condition at the rigid surface is

$$\frac{\partial\Phi_m(x,\xi,r,\hat{r})}{\partial r}=0 \quad \text{at } r=R. \tag{4b}$$

This formulation is equivalent to the following one

$$\frac{\partial^2\hat{\Phi}_m(x,\xi,r,\hat{r})}{\partial x^2}+\frac{1}{r}\frac{\partial\hat{\Phi}_m(x,\xi,r,\hat{r})}{\partial r}+\frac{\partial^2\hat{\Phi}_m(x,\xi,r,\hat{r})}{\partial r^2}+\left[\frac{\omega^2}{c_{\mathrm{fl}}^2}-\frac{m^2}{r^2}\right]\hat{\Phi}_m(x,\xi,r,\hat{r})=0. \tag{5a}$$

The loading condition is formulated as ($x\to\xi$)

$$\left.\frac{\partial\Phi_m(x,\xi,r,\hat{r})}{\partial x}\right|_{x=\xi}=\frac{1}{2\hat{r}}\delta(r-\hat{r})\mathrm{sgn}(x-\xi). \tag{5b}$$

This Green's function may be formulated in the form of a modal decomposition as

$$\Phi_m(x,\xi,r,\hat{r})=\sum_n D_{mn}(\hat{r})J_m\left(r\sqrt{k_n^2+\frac{\omega^2}{c_{\mathrm{fl}}^2}}\right)\exp(k_n|x-\xi|). \tag{6}$$

In this formula, k_n are roots of the classic dispersion equation

$$\left.\frac{\mathrm{d}}{\mathrm{d}r}\left[J_m\left(r\sqrt{k_n^2+\frac{\omega^2}{c_{\mathrm{fl}}^2}}\right)\right]\right|_{r=R}=0. \tag{7}$$

The coefficients $D_{mn}(\hat{r})$ are found from the following condition:

$$\sum_n k_n D_{mn}(\hat{r})J_m\left(r\sqrt{k_n^2+\frac{\omega^2}{c_{\mathrm{fl}}^2}}\right)=\frac{1}{2\hat{r}}\delta(r-\hat{r}). \tag{8}$$

Due to orthogonality of Bessel functions (κ_n, κ_k are the roots of dispersion equation (7) , $k\neq n$)

$$\int_0^1 J_m(\kappa_n r)\cdot J_m(\kappa_k r)r\,\mathrm{d}r=0, \tag{9}$$

each coefficient is found individually as

$$D_{mn}(\hat{r})=\frac{1}{2\hat{r}k_n Z_{mn}}J_m\left(\hat{r}\sqrt{k_n^2+\frac{\omega^2}{c_{\mathrm{fl}}^2}}\right),\quad Z_{mn}=\int_0^1\left[J_m\left(r\sqrt{k_n^2+\frac{\omega^2}{c_{\mathrm{fl}}^2}}\right)\right]^2 r\,\mathrm{d}r. \tag{10}$$

This formulation of Green's function is not very convenient for a detailed analysis of the acoustic pressure field in the excitation zone because the convergence of the series on Bessel functions to the prescribed 'δ-shape' is very slow. However, as soon as the energy transportation to the far field is concerned, the accuracy of a modal decomposition is entirely recovered. Indeed, in this purely acoustical wave-guide there are just a few propagating modes in the not-too-high frequency range, whereas the vast majority of the modes involved in decomposition (6) are evanescent. These non-propagating modes are essential in setting the 'δ-shape' of the real part of Green's function, but they do not contribute at all to its imaginary part. Moreover, due to orthogonal properties of Bessel functions, the amplitudes of propagating components are not influenced at all

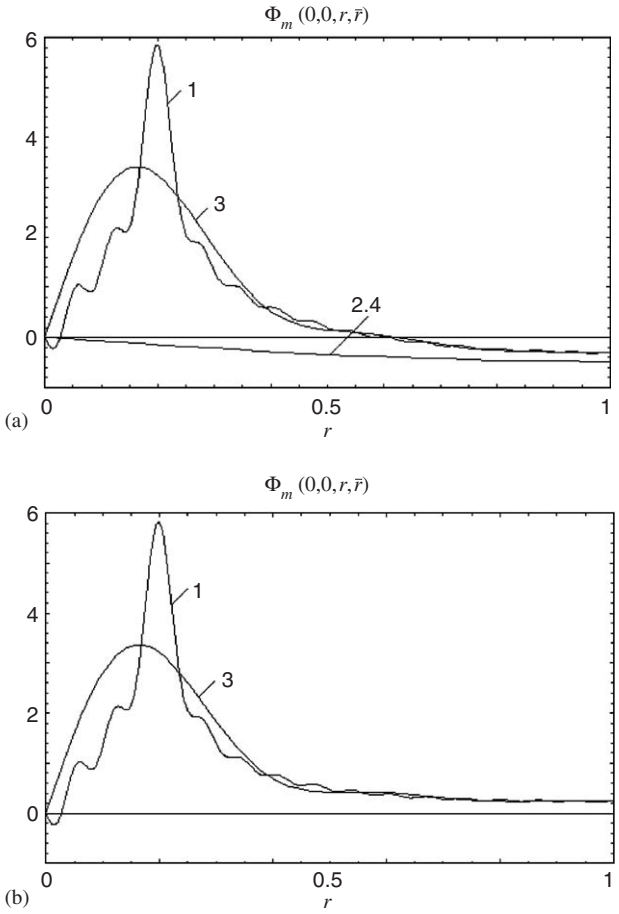

Fig. 1. The shape of Green's function $\Phi_m(0,0,r,\hat{r})$ for $m=1$, $\hat{r}=0.2$. (a) $\omega R/c_{\mathrm{fl}}=0.8$, (b) $\omega R/c_{\mathrm{fl}}=0.1$.

by the number of terms retained in Eq. (6). This way to formulate the Green's function presents, in effect, a modal decomposition of a 'ring source' concentrated in the radial direction.

As a simple example, the shape of Green's function $\Phi_m(0,0,r,\hat{r})$ is shown in Fig. 1a for $\omega R/c_{\mathrm{fl}}=0.8$, $m=1$, $\hat{r}=0.2$. Its real (curve 1) and imaginary (curve 2) are shown in the case, when 30 terms are retained in formula (6). Curves 3 and 4 present the same function approximated only by 6 terms in this formula. As is seen, there is a substantial difference in the shape of the real parts, whereas the imaginary part is the same in both cases. As shown in Fig. 1b, n the case $\omega R/c_{\mathrm{fl}}=0.1$, $m=1$, $\hat{r}=0.2$, the imaginary past does not exist (this frequency is below the first cut-on one), where as the real part does not differ much from the previous case at the both approximation levels. In fact, the real part of Green's function may be obtained accurately if a model of an incompressible fluid is used in this case. As discussed, the adequate approximation of the function $\delta(r-\hat{r})$ requires a very large number of terms in formula (6), but there is no contribution of all these high-order terms to the imaginary part of this Green's function. This simple result leads to the conclusion that for the purposes of analysis of the power flows the concept of modal Green's functions is applicable.

3.2. An elastic shell with heavy fluid loading

As is shown in the previous subsection, it is practical to use modal Green's functions and, as far as the energy generation is concerned, it is essential to take into account all components of Green's function which correspond to propagating modes at the given frequency. Then the set of loading conditions, which defines

modal acoustical Green's function is formulated as (for more details, see Refs. [9,10])

$$u^{\mathrm{ac}}_{mn}(x,\xi)=0,$$

$$Q^{\mathrm{ac}}_{2mn}(x,\xi)=-\frac{1-\nu}{2}\frac{m}{R}u^{\mathrm{ac}}_{mn}+\frac{1-\nu}{2}\frac{\partial v^{\mathrm{ac}}_{mn}}{\partial x}+\frac{h^2}{12}\frac{2(1-\nu)}{R^2}\frac{\partial v^{\mathrm{ac}}_{mn}}{\partial x}+\frac{h^2}{12}\frac{2(1-\nu)m}{R^2}\frac{\partial w^{\mathrm{ac}}_{mn}}{\partial x}=0,$$

$$Q^{\mathrm{ac}}_{3mn}(x,\xi)=-\frac{h^2}{12}\left[\frac{\partial^3 w^{\mathrm{ac}}_{mn}}{\partial x^3}-\frac{(2-\nu)m^2}{R^2}\frac{\partial w^{\mathrm{ac}}_{mn}}{\partial x}-\frac{(2-\nu)m}{R^2}\frac{\partial v^{\mathrm{ac}}_{mn}}{\partial x}\right]=0,$$

$$\frac{\partial w^{\mathrm{ac}}_{mn}(x,\xi)}{\partial x}=0,$$

$$\frac{\partial \varphi^{\mathrm{ac}}_{mn}(x,\xi,r)}{\partial x}=\frac{1}{2}\mathrm{sgn}\left(\frac{x-\xi}{R}\right)\psi_{mn}(r),\quad n=1,2,...,N. \tag{11}$$

Here the function $\psi_{mn}(r)$ is chosen as the nth eigenmode of the distribution of a velocity potential in the cross-section of a shell filled with a fluid,

$$\psi_{mn}(r)=J_m(\kappa_n r). \tag{12}$$

The modal Green's functions are more convenient, than a 'genuine' one as long as the energy transportation in an infinitely long fluid-filled shell is concerned. The solution is sought as

$$u^{\mathrm{ac}}_{mn}(x,\xi)=\mathrm{sgn}\left(\frac{x-\xi}{R}\right)\sum_{j=1}^{M}\alpha_j C^{\mathrm{ac}}_{jn}\exp\left(\frac{k_j}{R}|x-\xi|\right),$$

$$v^{\mathrm{ac}}_{mn}(x,\xi)=\sum_{j=1}^{M}\beta_j C^{\mathrm{ac}}_{jn}\exp\left(\frac{k_j}{R}|x-\xi|\right),\quad w^{\mathrm{ac}}_{mn}(x,\xi)=\sum_{j=1}^{M}C^{\mathrm{ac}}_{jn}\exp\left(\frac{k_j}{R}|x-\xi|\right),$$

$$\varphi^{\mathrm{ac}}_{m}(x,\xi,r)=\sum_{j=1}^{M}-\mathrm{i}\omega\, C^{\mathrm{ac}}_{jn}J_m(\kappa_j r)\left(\frac{\mathrm{d}J_m(\kappa_j r)}{\mathrm{d}r}\bigg|_{r=R}\right)^{-1}\exp\left(\frac{k_j}{R}|x-\xi|\right), \tag{13}$$

$$\kappa_j^2=\left(\frac{k_j}{R}\right)^2+\left(\frac{\omega}{c_{\mathrm{fl}}}\right)^2.$$

In Eqs. (12,13), k_j are roots of dispersion equation for a shell filled with fluid. The number of terms in modal expansions (13) may be relatively small as long as the energy transmission in a low-frequency range (i.e., below the 'ring frequency' of an empty shell, $\omega_{\mathrm{ring}}R/c_{\mathrm{sh}}=1$) is concerned. Just one or two propagating waves exist in this wave-guide for the not-too-high frequency range. Then it is sufficient to retain the full set of 'structure-originated' modes (there are always four of them) and add just 1–3 'fluid-originated' ones. The methodology of setting up the system of linear algebraic equations to find the coefficients C^{ac}_{nj} is fairly straightforward and it is reported in Ref. [9].

Unlike the case of a rigid tube, the Bessel's functions $J_m(\kappa_n r)$ satisfy the generalised orthogonality condition, which involves structural components in this case, rather than the 'conventional' condition (9). Thus, an aspect of convergence needs to be discussed. A copper shell ($\rho_{\mathrm{sh}}=8500\,\mathrm{kg/m^3}$, $E=2.1\times10^5\,\mathrm{MPa}$) of the thickness $h=1\,\mathrm{mm}$ and radius $R=14\,\mathrm{mm}$ filled with water ($\rho_{\mathrm{fl}}=1000\,\mathrm{kg/m^3}$, $c_{\mathrm{fl}}=1.5\times10^3\,\mathrm{m/s}$) is considered as an example. Computations with various numbers of modes retained in series (13) are performed for three types of mechanical excitation and for acoustical excitation. The acoustical excitation is formulated as a unit jump in velocity profile, which is distributed in the radial direction as $\psi_{m5}(r)=J_m(\kappa_1 r)$ at $\xi=0$ (here $\kappa_1=\sqrt{(k_1/R)^2+(\omega/c_{\mathrm{fl}})^2}$, k_1 is the wavenumber of the propagating mode). The ratio R_{power} of the total power input predicted in the cases, when 5, 6 and 7 terms are retained in formulas (13) to the power input predicted with 8 roots retained is presented in Table 1 for $m=1$, $f=800\,\mathrm{Hz}$.

Table 1
The total power predictions

No. of roots	8	7	6	5
Axial	1	1	1	1
Radial	1	0.98	0.87	0.82
Acoustical	1	0.965	0.84	0.80

4. Comparison of power inputs into elastic water-filled shell in different excitation conditions

To derive boundary integral equations for an arbitrary loaded elastic fluid-filled shell, a full Green's matrix should be used, which includes 'fundamental' mechanical and 'fundamental' acoustical excitation cases. However, before addressing sound generation and transmission in an inhomogeneous structure it is useful to compare the energy inputs and the energy distributions between alternative transmission paths in 'fundamental loading cases'.

Consider the shell of the same parameters as before vibrating at $m = 1$, $f = 800$ Hz. In Fig. 2, the distribution of the normalised energy flow between the structural and acoustical components is presented (computations are performed with $M = 7$) in the cases of (a) axial, (b) radial, (c) circumferential and (d) acoustical excitation. The energy flow is scaled by a half of the power input into the shell in the given excitation conditions. As is seen, the balance between the mechanical and the acoustical transmission in the far field is the same for all excitation cases. It is a fairly obvious result, which is readily explained by inspection into the wave-guide properties of a water-filled shell at this frequency. There exists only one structure-originated propagating wave and the energy distribution between transmission paths (including a distribution of the mechanical part between torsion, axial and flexural components of deformation of the wall of a shell) is uniquely defined regardless the excitation conditions. Perhaps, the less trivial conclusion derived from these graphs is the estimate of the length of a 'boundary layer', where the energy re-distribution actually takes place. It is remarkable that in the case of acoustical excitation (see Fig. 2d) almost all energy is 'trapped' in the dominantly structural wave within the distance of approximately one shell's diameter away from a loaded cross-section.

The methodology described in this section is equally applicable for analysis of wave motion at an arbitrary number of circumferential waves. In the case $m = 0$, purely torsion propagating wave in the shell is totally uncoupled with all others and it does not interact with an acoustic medium. Therefore, the formulation of Green's matrix at this circumferential wavenumber does not involve the circumferential displacement and the circumferential force.

In Fig. 3a–d, the distribution of normalised energy flow between the structural and acoustical components is presented for $m = 0$ in the cases of axial, radial and modal acoustical excitation. Unlike the previous case ($m = 1$), the balance between alternative transmission paths (including the distribution of the total structural part (curve 1) between longitudinal (curve 3) and flexural (curve 4) components) strongly depends on the excitation conditions. The acoustic component is designated by curve 2. The flexural component is presented only in Fig. 3b, because, as is seen from this figure, it almost vanishes within the distance of one radius from the excitation point. Then the magnitude of the total structural energy flow becomes the same as its longitudinal component.

In a case of the axial excitation (see Fig. 3a), the energy injected into the wall of a shell remains there almost entirely, with just 2% fluctuation due to the energy exchange with the acoustical component. These fluctuations are periodic. In Fig. 3b, the energy distribution in a near field is shown in the case, when a radial force is applied. As is seen, the energy, which is injected into the structure, leaves the wall of a shell within a very short distance from the excitation point. The structural energy flow is also transformed from the flexural deformation to the axial deformation. The far field energy distribution is illustrated in Fig. 3c. The 'averaged' proportion between the structural and the acoustical components may be estimated as 5% and 95%, respectively, with the fluctuations in 2%. Naturally, the length scale of these fluctuations is exactly the same as in the previous case. In the case of the modal acoustical excitation (Fig. 3d), the energy distribution may be

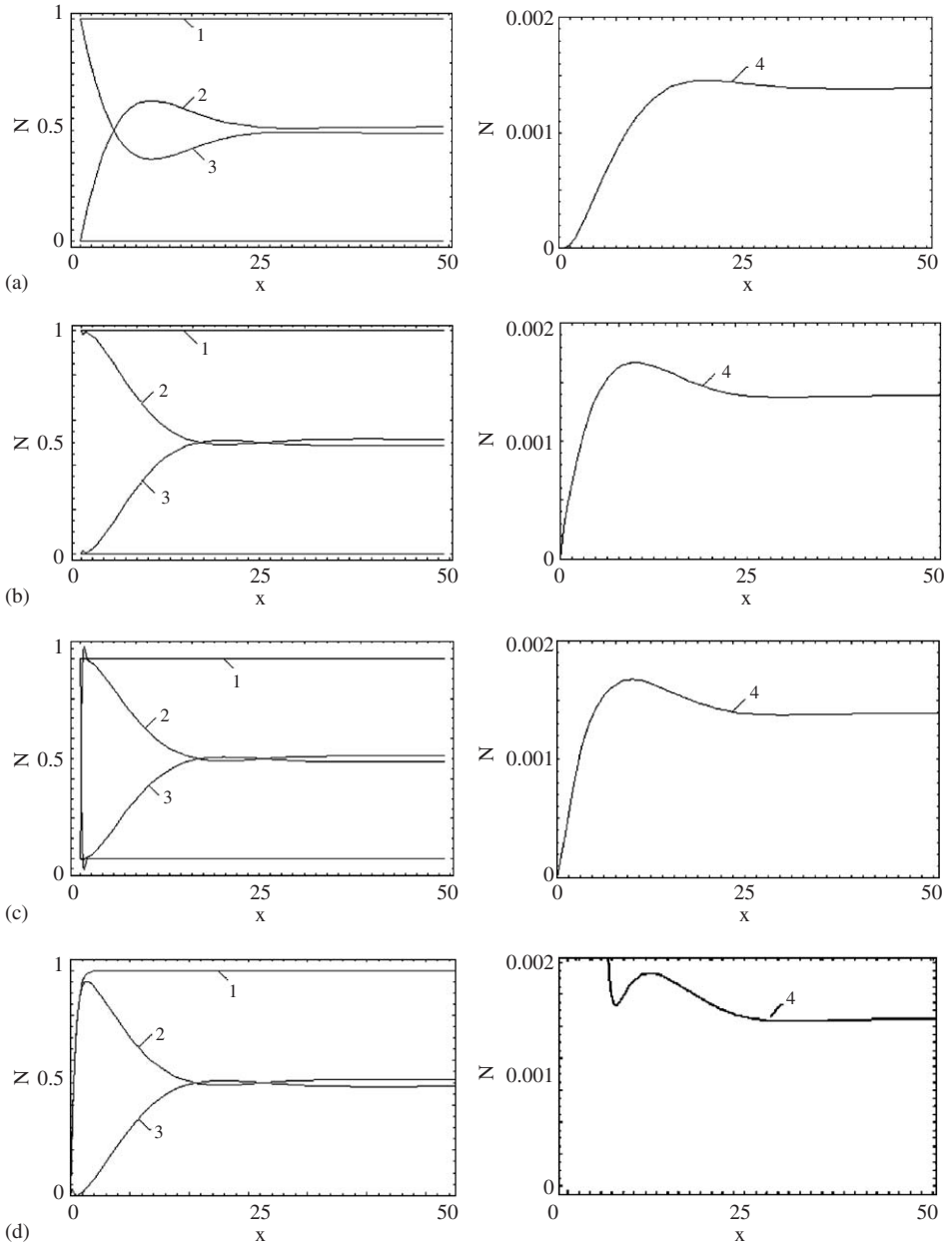

Fig. 2. The normalised energy flow, $m = 1$: (a) axial excitation; (b) circumferential excitation; (c) radial excitation; and (d) acoustical excitation.

regarded as a 'reversed case' of the axial excitation. In this situation, the most of energy flow does not leave an acoustic medium, where it has been injected.

In Figs. 2 and 3, the energy input is chosen as a scale to compare different components of the power flow in given excitation conditions. This interpretation has revealed the similarities in energy distribution in a far field in various excitation cases, but it has concealed the fact that to produce the same energy flow in the same water-filled shell at the same frequency, the amplitudes of axial, circumferential and radial forces and the amplitude of flow velocity pulsation are rather different. In the case of mechanical excitation, an intensity of force of any type distributed in circumferential direction has the dimension N/m and it is scaled by $Eh/(1-\nu^2)$. Thus it is a straightforward task to compare the efficiency of various types of excitation. In Fig. 4a, the ratio of

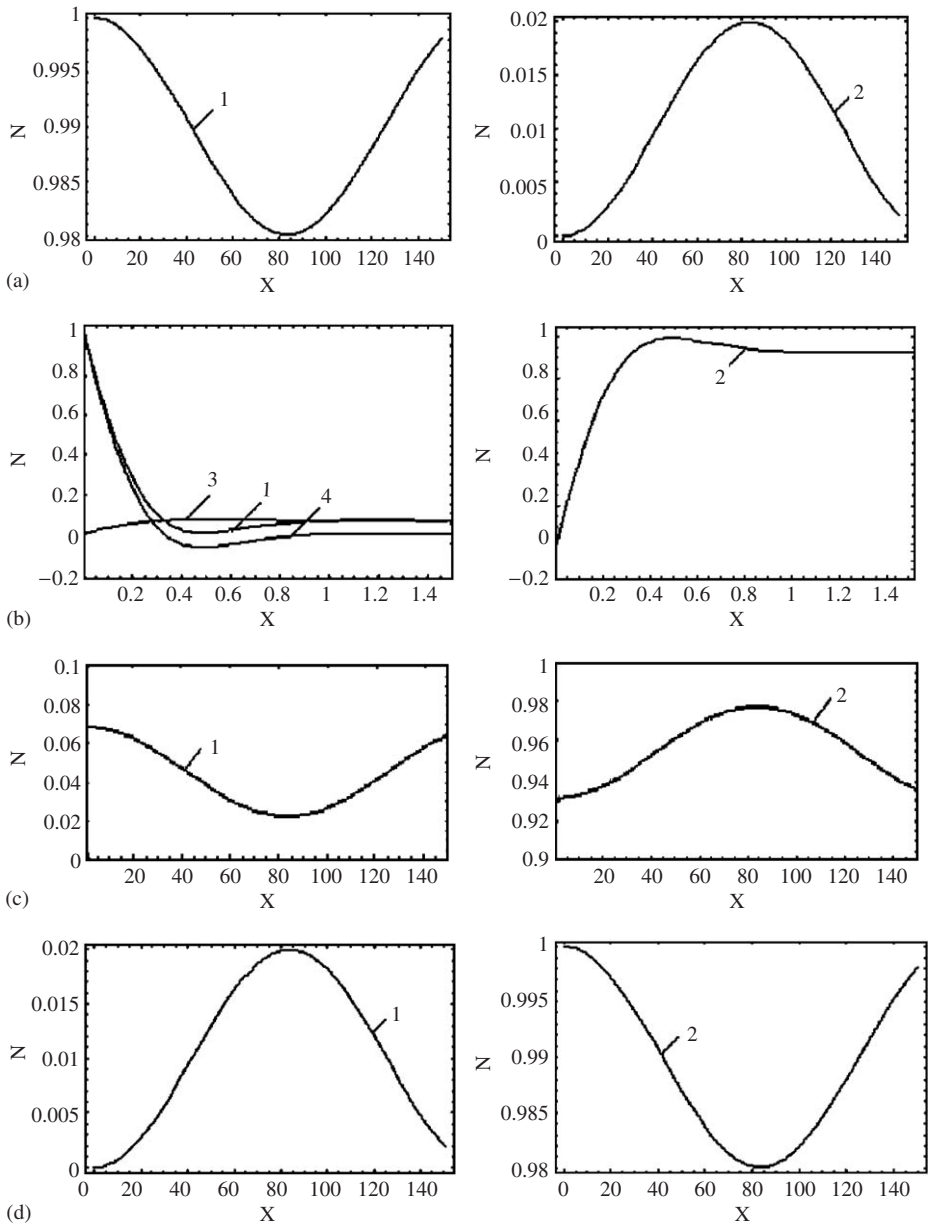

Fig. 3. The normalised energy flow, $m = 0$: (a) axial excitation; (b) radial excitation, near field; (c) radial excitation, far field; and (d) acoustical excitation.

the power input into the shell in the case of excitation by a circumferential force to the power input into the shell in the case of excitation by a radial force is presented versus frequency parameter for $m = 1$. As is seen, there is a very small difference between these power inputs in the whole frequency range. This result has an elementary physical explanation: in the relatively low-frequency range, the dynamics of a shell vibrating at the beam-type mode may be described within the simple beam theory. Then there is no difference between circumferential and radial loadings, which are replaced by the force resultant acting at a beam of the tubular cross-section. The progressive deviation of this ratio from unity with the growth in excitation frequency hints towards the approximation nature of this modelling. The ratio of the energy input by an axial force to the energy input by a radial force is shown in Fig. 4b. As is seen, the in-plane axial excitation is much less efficient at the considered mode. This may also be readily explained by the fact that axial force distributed in the

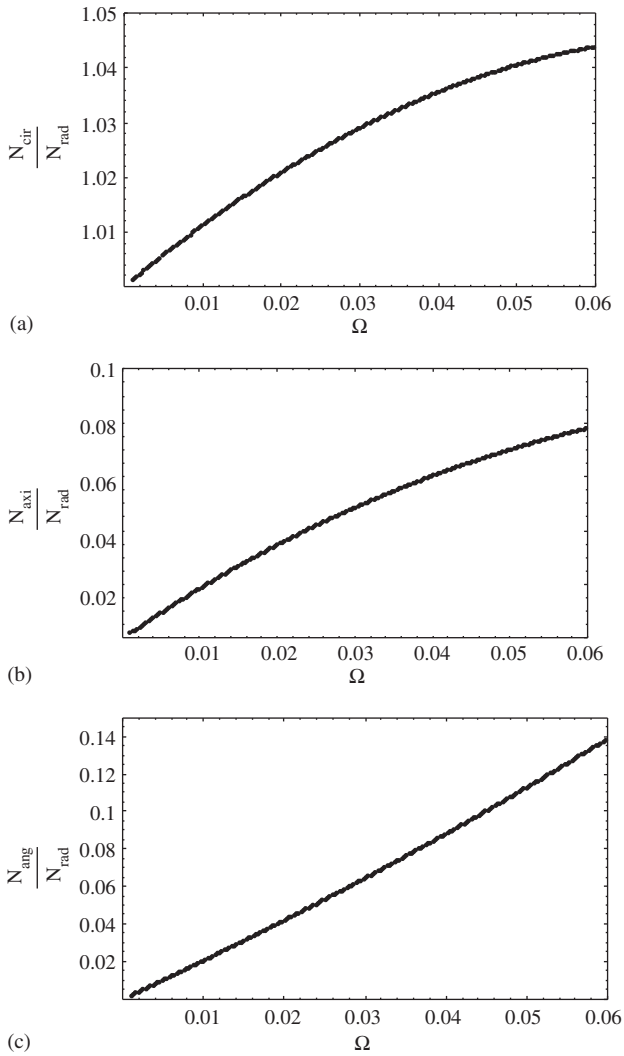

Fig. 4. Comparison of the efficiency of excitation, $m = 1$: (a) circumferential to radial; (b) axial to radial; and (c) angular to radial.

circumference as $\cos\theta$ does not produce any net force, but it does produce a net moment resultant. The axial excitation is less efficient than the radial and circumferential ones similarly to the lower radiation efficiency of dipoles as compared with monopoles in linear acoustics. For a reference, in Fig. 4c the ratio of the energy input by a distributed bending moment to the energy input by a radial force is shown. The curves in Figs. 4b, c have the same tangent as $\Omega \to 0$, but the excitation by the distributed bending moment becomes more efficient with the growth in frequency.

In the case of a breathing mode ($m = 0$), the efficiency of radial excitation is much lower than the efficiency of axial excitation, see Fig. 5. A net force is zero in a case of the radial excitation, but it is not zero for the axial excitation. It is less trivial to compare axial excitation with acoustical excitation, because the energy flow in the latter case is computed for a unit distributed force and in the latter case for a unit amplitude of velocity. Let the distributed force be of the amplitude 1N/m and let the amplitude of modal velocity fluctuation be 1m/s. The ratio of energy inputs produced in these two cases is very large and it is almost constant in the considered frequency range (it varies from $N_{ac}/N_{ax} = 9.544 \times 10^3$ at $\Omega = 0.001$ to $N_{ac}/N_{ax} = 9.536 \times 10^3$ at $\Omega = 0.06$). It should be noted that the amplitude of the force resultant for the tube of a radius of 14 mm equals 0.088 N. It is a very small force, whereas the amplitude of velocity fluctuation of 1m/s is very large indeed.

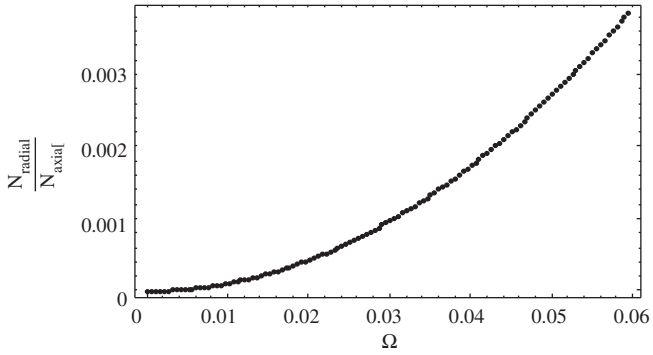

Fig. 5. Comparison of the efficiency of excitation, $m = 0$. Radial to axial.

5. Boundary integral equations for an elastic shell with heavy fluid loading

In the case of flow-induced vibrations of an elastic cylindrical shell filled with water, the 'sub-domain' methodology is conveniently applied. As already discussed, assume that the 'CFD volume' (a fluid's volume, where numerical solution of Navier–Stokes equations—including the pressure distribution at the rigid wall—is available) is confined: $x_{\min} < x < x_{\max}$. Furthermore, assume that all sources are located in this 'inner domain' (which consists of a shell and a fluid) and the 'outer domain' is free from any of them. As suggested by Lighthill's acoustic analogy, once the sources are identified in the inner domain the latter may be regarded as being filled with the same acoustic medium as outer domains. Then the boundary integral equations can be formulated for each of them. Due to modal decomposition in the circumferential coordinate, equations at each circumferential wavenumber are formulated separately and integration is performed analytically that reduces the integral equations to the algebraic form.

Boundary equations in this case involve both the acoustical and the structural variables. The Somigliana identity for the 'inner' domain of a cylindrical shell with heavy fluid loading is formulated as

$$
\begin{aligned}
&-\left[Q_{1m}^{0j}(x,\xi)u_m(x)+Q_{2m}^{0j}(x,\xi)v_m(x)+Q_{3m}^{0j}(x,\xi)w_m(x)+Q_{4m}^{0j}(x,\xi)w'_m(x)\right]\Big|_{x=x_{\min}}^{x=x_{\max}}\\
&\quad+\frac{\rho_{\mathrm{fl}}}{\rho}\frac{R}{h}\frac{(1-\nu^2)\rho\omega^2R^2}{E}\int_0^1\frac{\partial\varphi_m^{0j}(x,\xi,r)}{\partial x}\varphi_m(x,r)r\,\mathrm{d}r\Big|_{x=x_{\min}}^{x=x_{\max}}\\
&\quad-\delta_{1j}u_m(\xi)-\delta_{2j}v_m(\xi)-\delta_{3j}w_m(\xi)-\delta_{4j}w'_m(\xi)\\
&\quad-\delta_{nj}\frac{\rho_{\mathrm{fl}}}{\rho}\frac{R}{h}\frac{(1-\nu^2)\rho\omega^2R^2}{E}\int_0^1\psi_{jm}(r)\varphi_m(\xi,r)r\,\mathrm{d}r
\end{aligned}
$$

$$
\begin{aligned}
=&-\left[Q_{1m}(x)u_m^{0j}(x,\xi)+Q_{2m}(x)v_m^{0j}(x,\xi)+Q_{3m}(x)w_m^{0j}(x,\xi)+Q_{4m}(x)\frac{\partial w_m^{0j}(x,\xi)}{\partial x}\right]\Big|_{x=x_{\min}}^{x=x_{\max}}\\
&+\frac{\rho_{\mathrm{fl}}}{\rho}\frac{R}{h}\frac{(1-\nu^2)\rho\omega^2R^2}{E}\int_0^1\frac{\partial\varphi_m(x,r)}{\partial x}\varphi_m^{0j}(x,\xi,r)r\,\mathrm{d}r\Big|_{x=x_{\min}}^{x=x_{\max}}\\
&-\frac{\rho_{\mathrm{fl}}}{\rho}\frac{R}{h}(1-\nu^2)\int_{x_{\min}}^{x_{\max}}\int_0^1 i\frac{\Gamma^{(m)}(x,r)}{c_{\mathrm{shell}}^2}\varphi_m^{0j}(x,\xi,r)r\,\mathrm{d}r\,\mathrm{d}x-\frac{R}{h}\frac{(1-\nu^2)}{E}\int_{x_{\min}}^{x_{\max}}q_{3m}(x)w_m^{0j}(x,\xi)\,\mathrm{d}x. \qquad (14)
\end{aligned}
$$

The set of boundary equations is derived from this identity when the observation point ξ tends to the boundary from 'inside' of this domain. These boundary equations are formulated for unknown displacements $u(x)$, $v(x)$, $w(x)$, $w'(x)$ and forces $Q_j(x)$, $j = 1,2,3,4$ at the interfacial points $x = x_{\min}$ and $x = x_{\max}$ in the same way as they are formulated for a shell without fluid loading. However, due to the presence of fluid loading, identity (14) contains additional unknown functions $\varphi_m(x,r)$ and $\partial\varphi_m(x,r)/\partial x$ at $x = x_{\min}$ and $x = x_{\max}$. More

specifically, the convolutions

$$\int_0^1 J_m(\kappa_j r)\varphi_m(x,r)r\,\mathrm{d}r \quad \int_0^1 J_m(\kappa_j r)\frac{\partial\varphi_m(x,r)}{\partial x}r\,\mathrm{d}r, \quad j=1,...,M, \quad x=x_{\min}, \quad x=x_{\max} \tag{15}$$

are involved in the formulation of Eq. (14).

To obtain a well-defined formulation of boundary equations, the unknown velocity potential field at $x=x_{\min}$, $x=x_{\max}$ is sought in the form of a modal decomposition

$$\varphi_m(x_{\min},r)=\sum_{j=5}^{M}\lambda_{jm}(x_{\min})J_m(\kappa_j r), \quad \varphi_m(x_{\max},r)=\sum_{j=5}^{M}\lambda_{jm}(x_{\max})J_m(\kappa_j r),$$

$$\left.\frac{\partial\varphi_m(x,r)}{\partial x}\right|_{x=x_{\min}}=\sum_{j=5}^{M}\mu_{jm}(x_{\min})J_m(\kappa_j r), \quad \left.\frac{\partial\varphi_m(x,r)}{\partial x}\right|_{x=x_{\min}}=\sum_{j=5}^{M}\mu_{jm}(x_{\max})J_m(\kappa_j r). \tag{16}$$

Then convolutions (16) contain $4(M-4)$ algebraic unknowns $\lambda_{jm}(x_{\max})$, $\lambda_{jm}(x_{\min})$, $\mu_{jm}(x_{\max})$, $\mu_{jm}(x_{\min})$, $j=5,\ldots,M$. The overall number of unknowns involved in the problem formulation for the 'inner' domain is $4M$, whereas the number of boundary equations is $2M$ (there are M boundary equations, which follow from identity (14) for $x=x_{\min}$ and $x=x_{\max}$.

The similar formulation is available for the two semi-infinite 'outer' domains, however the unknowns are introduced just at their interfaces with the 'inner' domain. Specifically, for the domain $-\infty<x<x_{\min}$ the identity is formulated as

$$\begin{aligned}
&-Q_{1m}^{0j}(x_{\min},\xi)u_m(x_{\min})-Q_{2m}^{0j}(x_{\min},\xi)v_m(x_{\min})-Q_{3m}^{0j}(x_{\min},\xi)w_m(x_{\min})\\
&-Q_{4m}^{0j}(x_{\min},\xi)w_m'(x_{\min})+\frac{\rho_{\mathrm{fl}}}{\rho}\frac{R}{h}\frac{(1-\nu^2)\rho\omega^2R^2}{E}\int_0^1\frac{\partial\varphi_m^{0j}(x,\xi,r)}{\partial x}\varphi_m(x,r)r\,\mathrm{d}r|_{x=x_{\min}}\\
&\qquad-\delta_{1j}u_m(\xi)-\delta_{2j}v_m(\xi)-\delta_{3j}w_m(\xi)-\delta_{4j}w_m'(\xi)\\
&\qquad-\delta_{nj}\frac{\rho_{\mathrm{fl}}}{\rho}\frac{R}{h}\frac{(1-\nu^2)\rho\omega^2R^2}{E}\int_0^1\psi_{jm}(r)\varphi_m(\xi,r)r\,\mathrm{d}r\\
=\;&-Q_{1m}(x_{\min})u_m^{0j}(x_{\min},\xi)-Q_{2m}(x_{\min})v_m^{0j}(x_{\min},\xi)-Q_{3m}(x_{\min})w_m^{0j}(x_{\min},\xi)\\
&-Q_{4m}(x_{\min})\left.\frac{\partial w_m^{0j}(x,\xi)}{\partial x}\right|_{x=x_{\min}}+\frac{\rho_{\mathrm{fl}}}{\rho}\frac{R}{h}\frac{(1-\nu^2)\rho\omega^2R^2}{E}\int_0^1\frac{\partial\varphi_m(x,r)}{\partial x}\varphi_m^{0j}(x,\xi,r)r\,\mathrm{d}r\Bigg|_{x=x_{\min}}.
\end{aligned} \tag{17}$$

Its counterpart for the domain $x_{\max}<x<\infty$ has the same form, but $x_{\min}$ is replaced by $x_{\min}$ and all the terms, which contain the factor $\delta-$ function, have the sign plus. No loading terms are included in Eq. (17) because the 'outer' domains are free from any excitation.

There are $2M$ with $4M$ unknowns for the both 'outer' domains together. At this stage, the system of algebraic equations consists of $4M$ equations with $8M$ unknowns. The continuity conditions should be formulated at the interfaces between the 'inner' and 'outer' domains $x=x_{\min}$ and $x=x_{\max}$. They involve the continuity of the amplitudes of displacements and forces at the 'structural' interface (eight conditions at each interface) and the continuity of velocity potentials and their axial derivatives at the 'acoustical' interface. The latter are formulated in the integral form

$$\int_0^1 J_m(\kappa_j r)\left[\varphi_m^{\mathrm{in}}(x,r)-\varphi_m^{\mathrm{out}}(x,r)\right]r\,\mathrm{d}r=0,$$

$$\int_0^1 J_m(\kappa_j r)\left[\frac{\partial\varphi_m^{\mathrm{in}}(x,r)}{\partial x}-\frac{\partial\varphi_m^{\mathrm{out}}(x,r)}{\partial x}\right]r\,\mathrm{d}r=0 \;\; j=5,...,M. \tag{18}$$

These conditions give $4M$ additional equations at each interface. Therefore, a complete set of $8M$ linear algebraic equations is obtained.

The last two integrals on the right-hand side of Eq. (14) must be computed in the 'inner' domain. This step is computationally cheap for the last term in Eq. (14), but it is extremely expensive with respect to the volume sources $\Gamma^{(m)}$. It is advantageous to apply integration by parts to the double integral. This step in solution is particularly useful because the function $\Gamma^{(m)}$ is available only in a tabular form and its differentiation cannot be accurately calculated numerically. The integral over the surface of a shell presents the additional terms, which should be added to the mechanical excitation, the integrals over the interfaces $x = x_{\min}$ and $x = x_{\max}$ present the contribution of 'quadrupoles'. The residual volume integral is asymptotically small and may be neglected. Thus, the amount of CFD output data needed to perform vibro-acoustic analysis is substantially reduced. All volume sources are mapped onto the surface of a tube and onto interfaces between the 'inner' and the 'outer' domains. The location of the boundary between the 'inner' and the 'outer' domain should be defined in the 'euristic' way.

The system of boundary equations, derived in this section, is also applicable to consider wave propagation in a compound fluid-filled cylindrical shell, e.g., composed by segments with different stiffness, density or thickness. In such a case, the roots of dispersion equation should be found for each segment of a fluid-filled shell and the continuity conditions are formulated as outlined in Ref. [10].

6. Numerical examples

At sufficiently low frequencies, it is reasonable to assume that the pressure fluctuations produced by a flow obstacle are transmitted to the shell's wall as if water is incompressible. This assumption is very practical as far as an input data is taken from some CFD computations, because the amount of data transferred from a flow analysis to a vibro-acoustic power flow analysis is reduced very substantially in comparison with the total output of a CFD code. As already mentioned, this simplification is consistent with the fact that CFD codes operate with a 'rigid wall' conditions for a semi-confined fluid's volume.

It presents serious difficulties to obtain a numerical solution of the three-dimensional problem of a stationary flow of water in a tube with an obstacle, which may have a rather complicated shape of, say, a valve, and which is located not necessarily at the axis of a tube. On the other hand, it is well known that in the classical cases of sound generation by acoustically compact sources, a dipole source may successfully replace the 'physical obstacle'. The methodology suggested in this paper is illustrated in the following way. Firstly, to mimic the CFD output data, a pressure field at the surface of a rigid tube produced by generic time harmonic 'dipole sources' in an incompressible fluid is obtained in the form of modal Green's functions as outlined in Section 3. Secondly, this pressure field is applied as a mechanical excitation of an elastic cylindrical shell filled with a compressible fluid (water). This pressure is truncated to the segment $x_{\min} < x < x_{\max}$ (the 'inner domain') and it is set to zero at the shell's wall in the 'outer domain'. Then the power flow is computed. Furthermore, the 'inner domain' is extended to take into account for some additional sources and the energy flow calculation is repeated. A size of the 'inner domain', where most of the vibro-acoustic energy is generated, is assessed in this procedure.

6.1. Axi-symmetric 'ring dipole source'

Consider an axi-symmetric ring of dipole sources located in an absolutely rigid tube at the distance $r_{\text{ex}} = 0.5$ from its axis with a circumferential intensity of $1/r_{\text{ex}}$. The orientation of these dipoles is along the axis of a shell. In a far field, this 'ring source' can be viewed also as a dipole lying at the axis of a tube. It is assumed that the pressure field produced by these 'dipoles' is taken in the 'incompressible fluid' limit. It should be pointed out that such a problem formulation of its own right is physically correct: inasmuch a net volume source is zero, the pressure field decays sufficiently fast at infinity to ensure that the energy of fluid is bounded. The modal Green's function for the monopole ring source is derived in Section 3 for the case of compressible fluid. The formulation of dipole sources is obtained by differentiation of Eq. (6) in the coordinate of the source point ξ and then taking the limit of an incompressible fluid.

As has already been discussed, the pressure exerted by this ring source at the surface of a tube is taken as the mechanical excitation of a elastic tube filled with a compressible fluid. The excitation at the frequency $f = 800\,\text{Hz}$ of a shell ($h = 1\,\text{mm}$, $R = 1\,\text{mm}$, $\rho_{\text{sh}} = 8500\,\text{kg/m}^3$, $E = 2.1 \times 10^5\,\text{MPa}$) filled with water is

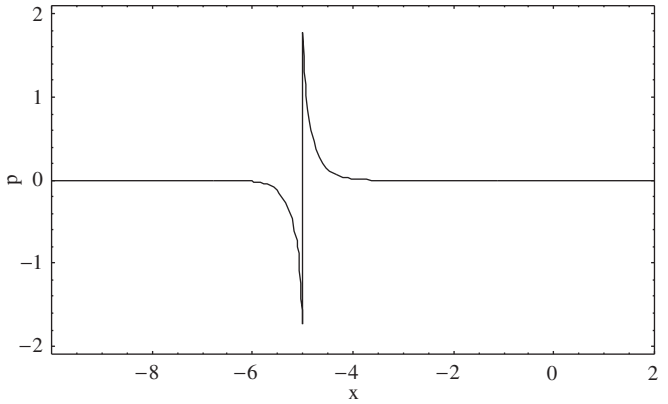

Fig. 6. 'Axi-symmetric ring dipole source', the distribution of scaled contact pressure.

considered. The distribution of scaled contact pressure at the inner surface of a shell in the axial direction is shown in Fig. 6. The negative values of the pressure to the left from the loaded point mean that it is always in the anti-phase with the pressure at the same distance to the right. The source is located at the point $\xi = -5$. As is seen, the pressure decays very rapidly as the distance increases.

In Fig. 7, the energy flow in a fluid-filled shell is shown as a function of distance. Fig. 7a is plotted in the case, when the 'inner domain' (where the pressure is read) is extended as $-6 \leqslant x \leqslant -4$. The graph in Fig. 7b is plotted for the 'inner domain' of $-9 \leqslant x \leqslant -1$. It is worth to notice that, although the mechanical excitation of a shell is considered, all energy actually returns to the fluid. This result to some extend justifies the concept of analysis used in this paper. Indeed, the 'originally' acoustical excitation (a ring dipole source) inside the tube is replaced by the mechanical excitation at its wall, which is provoked by the source. However, this mechanical excitation generates a dominantly acoustical wave and the resulting power flow is also dominantly acoustical. This issue has also been discussed in Section 4. It should be observed that the 'inner domain' is very compact and its extension yield an insignificant correction to the power flow. However, from the viewpoint of possible use of CFD codes, such an extension means a substantial increase in the required resources.

6.2. *Skew–symmetric 'ring monopole source'*

Consider as another 'generic' example a ring of monopole sources located in an absolutely rigid tube at the distance $r_{ex} = 0.5$ from its axis with a circumferential intensity of $\cos\theta/r_{ex}$. In a far field, this source can be viewed also as a dipole (see the previous case), but its axis is perpendicular to the axis of a tube. In Fig. 8, the pressure distribution generated by this source at the surface of a shell is shown. In this case, a non-zero time harmonic net force is produced and, as discussed in Section 3, the energy transmission is almost purely structural, with the dominant contributions of two in-plane components. So, unlike the previous case, the energy injected acoustically is transmitted to the far field through the structure, rather than through a fluid (this effect has also been discussed in Section 4).

As is seen from Fig. 9, the truncation of the 'inner domain' to $-6 \leqslant x \leqslant -4$ (curve 1) results in a larger error, than in the previous case. However, the difference between the cases $-7 \leqslant x \leqslant -3$ (curve 2) and $-9 \leqslant x \leqslant -1$ (curve 3) is insignificant. This result is rather trivial—the decay rate of a monopole source is known to be slower than of a dipole one. In this case, pressure distribution at the surface of a shell is defined analytically, and it is possible to replace the pressure distribution by a point radial force. The power flow produced by the radial force resultant of the pressure shown in Fig. 8 versus distance is shown by curve 4.

As is seen, there is a fundamental difference between the energy transmissions in the reported generic excitation cases. In the former case ('an axi-symmetric ring dipole source'), the methodology suggested in this paper might not be very useful—if the issues of transformation of CFD data are not tackled. The originally

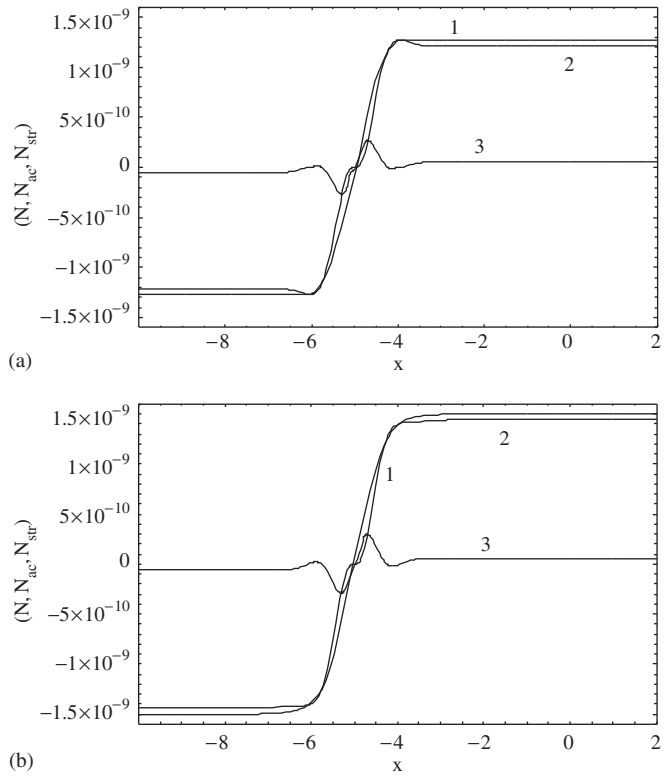

Fig. 7. The energy flow components: 1, total flow; 2, acoustical component; 3, structural component. (a) The 'inner domain' $-6 \leqslant x \leqslant -4$ and (b) the 'inner domain' $-9 \leqslant x \leqslant -1$.

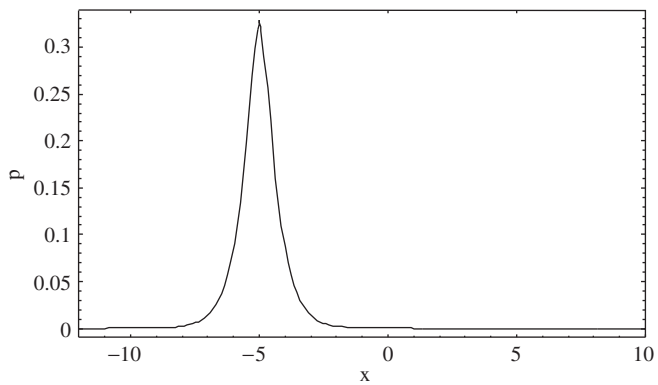

Fig. 8. 'Skew-symmetric ring monopole source', the distribution of scaled contact pressure.

acoustic excitation is transformed to mechanical excitation and the latter generates a dominantly acoustic power flow. Possibly, in this case a model of acoustic duct could be used. In the latter case ('a ring monopole source at $m = 1$'), the role of wave-guide properties of an elastic shell is crucial. The acoustical excitation generates dominantly structural power flow and a model of acoustic duct is not acceptable. This result is rather general and it is of particular importance in the low-frequency excitation cases. As is well known, the mode $m = 1$ has a non-zero cut-on frequency in an acoustic duct, whereas this mode in an elastic shell (a beam-type mode) propagates at any frequency and at low frequencies the role of compressibility of a fluid is negligible. Thus, the methodology suggested in this paper suits this case.

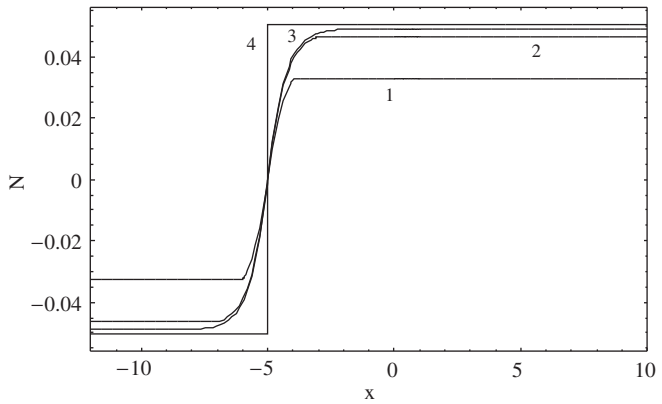

Fig. 9. The total energy flow: 1, the 'inner domain' $-6 \leqslant x \leqslant -4$; 2, the 'inner domain' $-9 \leqslant x \leqslant -1$; 3, the 'inner domain' $-9 \leqslant x \leqslant -1$; 4, the point force.

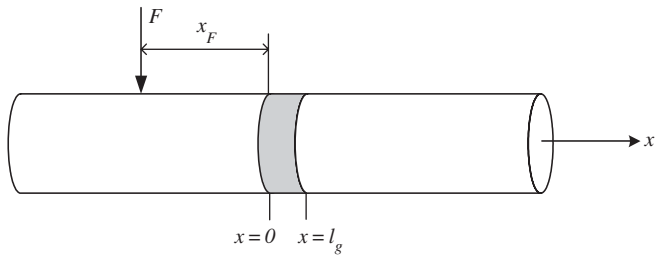

Fig. 10. A compound shell.

6.3. Compound shell and quadrupoles

As is mentioned in Section 5, the presence of quadrupole sources and the effects of discontinuities in characteristics of the shell (the case of a compound shell) may be conveniently treated by the use of boundary integral equations. Possibly, the contribution of quadrupoles is not too much pronounced at the low frequencies. However, the discontinuity effects may play a significant role in the energy transmission. As a simple illustrative example, consider an inhomogeneous shell, in which the inner and the outer domains are different due to the difference in the Young's module of segments of a shell (see Fig. 10). In this figure the point force marks the symmetry axis of the pressure distribution, which is actually shown in Fig. 8. The length of an insert equals the radius of a shell, it has the same thickness, but its Young's module may vary as follows: $0.01 \leqslant \gamma \equiv E_{\text{in}}/E \leqslant 1$. The excitation is produced by 'a ring monopole source at $m = 1$' (the second case considered earlier in this section) in the same shell at the same frequency. The location of an insert is fixed as $x_F = 0$, see Fig. 10. The computations are carried out with the 'inner domain' of $-9 \leqslant x \leqslant -1$.

Naturally, in the case, when parameters of the insert are identical to those of the main shell, the power flows to the right (N_1) and to the left (N_2) from the excitation zone are identical. Their magnitudes are presented in Fig. 11a by the point at $\gamma = 1$. As seen from this graph, 'weakening' of the insert results in an uneven distribution of the energy flow (the power flow through the insert increases), whereas the total power input remains approximately the same (down to $\gamma > 0.8$). A further decrease in Young's module of the insert's material results in a significant drop in the power injected into the shell and, in particular, in the power flow in the direction opposite to the insert. However, as the inclusion becomes very weak (see Fig. 11b), the power flows in both directions increase again and overshoot their magnitudes in the original homogeneous

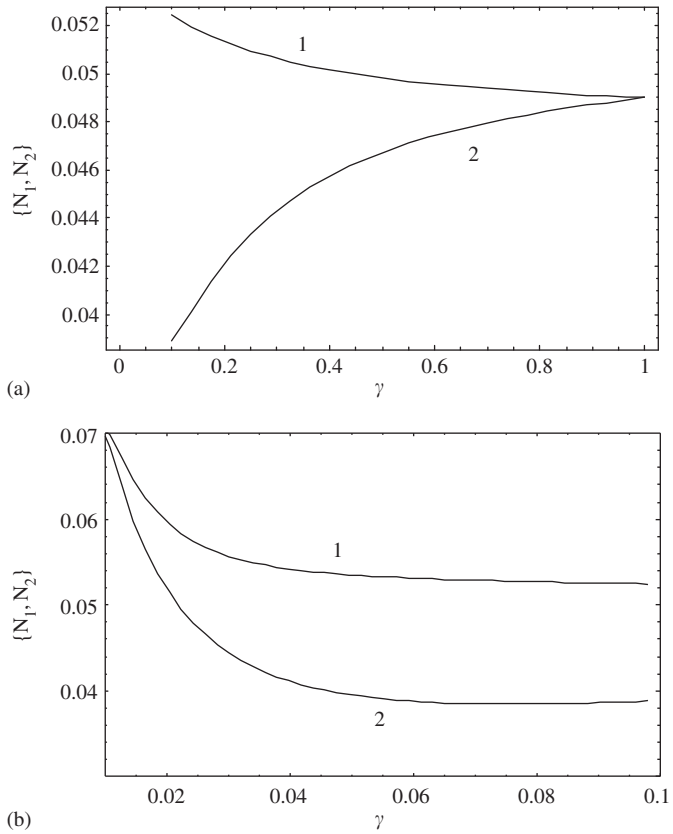

Fig. 11. The energy flows in the compound shell to the right (N_1) and to the left (N_2) from the excitation zone (a) $0.1<\gamma<1$, (b) $0.01<\gamma<0.1$.

structure. Such a complicated non-monotonous behaviour of this function is readily explained by interference effects of the direct waves produced by the pressure distributed as shown in Fig. 8 and the waves reflected at the junction sections, see Fig. 10. This illustrative example suggests that the method of boundary integral equations may also be applied to study and control the energy flows in compound fluid-filled elastic cylindrical shells.

7. Conclusions

A methodology of analysis of generation and transmission of vibro-acoustic energy in an elastic tube with heavy internal fluid loading is suggested and exemplified.

The methodology is summarised as follows:

- The energy generation is considered on the assumption that the back-reaction of the acoustic/structural response on the driving turbulent field is negligible. Then the flow-induced coupled vibro-acoustic field in an elastic cylindrical shell filled with water may be analysed as a forced response of this shell with internal heavy fluid loading to mechanical excitation, which is determined by pressure pulsations at its inner surface. Pressure pulsations may be found as a numerical solution of the problem in flow of an incompressible fluid in a rigid tube with a given obstacle inside. Hence, the presence of this obstacle as a dipole source should be ignored to avoid 'double counting' of the excitation sources.
- The boundary integral equations method is used to analyse transmission of the flow-induced sound and vibration. The modal boundary integral equations are derived, which are equally applicable to study the

wave propagation in homogeneous and in compound infinitely long elastic fluid-filled tubes in arbitrary excitation conditions. As a pre-requisite for these studies, Green's matrix is obtained.

The results of power flow analysis in the 'fundamental' mechanical and acoustical excitation cases (described by the Green's matrix of a fluid-filled shell) suggest that in an elastic water-filled shell vibrating at a relatively low frequency (the case relevant to many practical applications) the energy is transmitted mainly through the structure. Specifically, the 'structure-borne' sound dominates the 'fluid-borne' sound for the 'beam'-type mode $m = 1$ in any excitation conditions. However, in a 'breathing mode' $m = 0$ the energy distribution is case-sensitive and the 'fluid-borne' sound dominates the 'structure-borne' one in some circumstances highlighted in the paper. Although this energy distribution pattern is well known, the aspect of novelty of the reported results is presented by an estimate of the actual length of the 'boundary layer' along the tube, in which the far-field energy balance is set up. Another aspect of novelty is contained in comparison of the efficiency of various mechanical and acoustical 'fundamental' (i.e., those used in derivation of Green's matrix) excitations. The coupled vibro-acoustic response of a fluid-filled shell is studied in the two generic cases of acoustical excitation aimed to mimic the actual excitation by flow-induced pulsations. Although the considered cases are very different from each other regarding mechanisms of the energy transportation, the suggested methodology is able to capture the principal features of this phenomenon. Finally, the energy transportation in a compound shell is addressed and the role of discontinuities in parameters of a tube in re-distribution of the energy flows is highlighted.

Acknowledgements

Professor S.V. Sorokin expresses his sincere gratitude to Professor C.J. Chapman (Keele University, UK) and to Dr. B.O. Olsen (Sonion Horsens A/S, Denmark) for many inspiring discussions. The financial support provided to Dr. A.V. Terentiev by the Aalborg University is also gratefully acknowledged. The encouraging support and valuable advices from Professor C.L. Morfey are highly appreciated.

Appendix

The displacements of a shell element are shown in Fig. A1a. The force and moment resultants in a cross-section of the shell (see Fig. A1b), which are involved in the boundary and continuity conditions, are defined as (see Refs. [9,10]):

$$Q_{1m} = \frac{Eh}{1-\nu^2}\left(\frac{\mathrm{d}u_m}{\mathrm{d}x} + \frac{m\nu}{R}v_m + \frac{\nu}{R}w_m\right), \tag{A.1a}$$

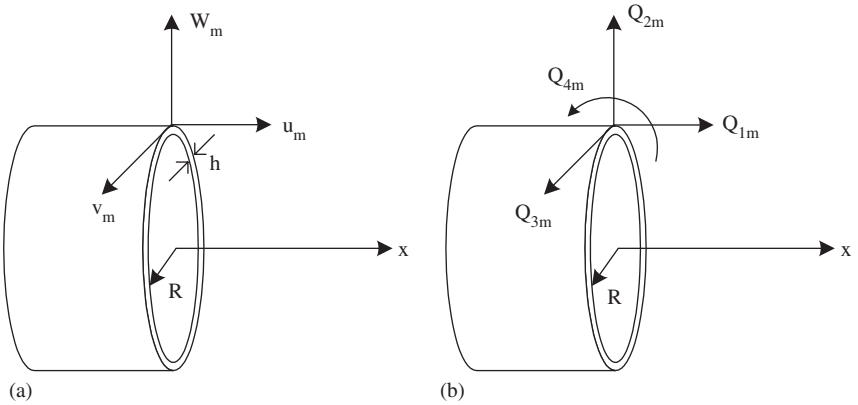

Fig. A1. A cylindrical shell: (a) modal displacements and (b) generalised modal forces.

$$Q_{2m} = \frac{Eh}{1-\nu^2}\left(-\frac{1-\nu}{2}\frac{m}{R}u_m + \frac{1-\nu}{2}\frac{\mathrm{d}v_m}{\mathrm{d}x} + \frac{h^2}{12}\frac{2(1-\nu)}{R^2}\frac{\mathrm{d}v_m}{\mathrm{d}x} + \frac{h^2}{12}\frac{2(1-\nu)m}{R^2}\frac{\mathrm{d}w_m}{\mathrm{d}x}\right), \tag{A.1b}$$

$$Q_{3m} = -\frac{Eh^3}{12(1-\nu^2)}\left[\frac{\mathrm{d}^3 w_m}{\mathrm{d}x^3} - \frac{(2-\nu)m^2}{R^2}\frac{\mathrm{d}w_m}{\mathrm{d}x} - \frac{(2-\nu)m}{R^2}\frac{\mathrm{d}v_m}{\mathrm{d}x}\right], \tag{A.1c}$$

$$Q_{4m} = \frac{Eh^3}{12(1-\nu^2)}\left[\frac{\mathrm{d}^2 w_m}{\mathrm{d}x^2} - \frac{m^2\nu}{R^2}w_m - \frac{m\nu}{R^2}v_m\right]. \tag{A.1d}$$

These formulas present the axial 'membrane' force, the circumferential 'membrane' force, the radial shear force and the axial bending moment, respectively.

The energy flow components are [9]

$$N_{m,\mathrm{out}}^{\mathrm{axial}} = -\gamma\pi R\frac{\omega}{2}\frac{Eh}{(1-\nu^2)}\left[\mathrm{Im}(u_m)\mathrm{Re}\left(Q_{1m}\right) - \mathrm{Re}(u_m)\mathrm{Im}\left(Q_{1m}\right)\right],$$

$$N_{m,\mathrm{out}}^{\mathrm{torsion}} = -\gamma\pi R\frac{\omega}{2}\frac{Eh}{(1-\nu^2)}\left[\mathrm{Im}(v_m)\mathrm{Re}\left(Q_{2m}\right) - \mathrm{Re}(v_m)\mathrm{Im}\left(Q_{2m}\right)\right],$$

$$\begin{aligned} N_{m,\mathrm{out}}^{\mathrm{bending}} = & -\gamma\pi R\frac{\omega}{2}\frac{Eh}{(1-\nu^2)}\left[\mathrm{Im}(w_m)\mathrm{Re}\left(Q_{3m}\right) - \mathrm{Re}(w_m)\mathrm{Im}\left(Q_{3m}\right)\right], \\ & -\gamma\pi R\frac{\omega}{2}\frac{Eh}{(1-\nu^2)}\left[\mathrm{Im}\left(w'_m\right)\mathrm{Re}\left(Q_{4m}\right) - \mathrm{Re}\left(w'_m\right)\mathrm{Im}\left(Q_{4m}\right)\right], \end{aligned}$$

$$N_{m,\mathrm{out}}^{\mathrm{fluid}} = -\gamma\frac{\pi\omega}{2}\int_0^R\left[\mathrm{Im}\left(p_m\right)\mathrm{Re}\left(\frac{\partial\varphi_m}{\partial x}\right) - \mathrm{Re}\left(p_m\right)\mathrm{Im}\left(\frac{\partial\varphi_m}{\partial x}\right)\right]r\,\mathrm{d}r, \tag{A.2}$$

where $\gamma = 2$ if $m = 0$ and $\gamma = 1$ if $m \neq 0$.

The total energy flow may then be formulated as

$$N_{m,\mathrm{out}}^{\mathrm{tot}} = N_{m,\mathrm{out}}^{\mathrm{axial}} + N_{m,\mathrm{out}}^{\mathrm{torsion}} + N_{m,\mathrm{out}}^{\mathrm{bending}} + N_{m,\mathrm{out}}^{\mathrm{fluid}}. \tag{A.3}$$

References

[1] P. Sagaut, E. Manoha (Eds.), *Euromech Colloquium 449 Computational Aeroacoustics: from Acoustic Source Modelling to Far-field Radiated Noise Predictions Proceedings*, 2003.

[2] C.L. Morfey, Fundamental problems in aeroacoustics, *Proceedings of the Seventh ICSV*, Vol.1, 2000, pp. 59–74.

[3] M.J. Lighthill, On sound generated aerodynamically. I. General theory, *Proceedings of the Royal Society* A 211 (1952) 564–587.

[4] A.L. Gol'denveiser, V.B. Lidskij, P.E. Tovstik, *Free Vibrations of Thin Elastic Shells*, Nauka, Moscow, 1929 (in Russian).

[5] N. Curle, The influence of solid boundaries upon aerodynamic sound, *Proceedings of the Royal Society* A 231 (1955) 505–514.

[6] M.S. Howe, *Acoustics of Fluid–Structure Interactions*, Cambridge University Press, Cambridge, MA, 1998.

[7] B. Olsen, Vibroacoustic Power Flow in Infinite Compliant Pipes Excited by Mechanical Force and Internal Acoustic Sources, PhD Thesis, ISVR, University of Southampton, UK, 2000.

[8] C.J. Chapman, private communication.

[9] S.V. Sorokin, J. Balle Nielsen, N. Olhoff, Green's matrix and the boundary integral equations method for analysis of vibrations and energy flows in cylindrical shells with and without internal fluid loading, *Journal of Sound and Vibration* 271 (2004) 815–847.

[10] S.V. Sorokin, O.A. Ershova, Analysis of the energy transmission in compound cylindrical shells with and without internal heavy fluid loading by boundary integral equations and by Floquet theory, *Journal of Sound and Vibration* 291 (2006) 81–99.